Dyes and Pigments 87 (2010) 164–172

Contents lists available at ScienceDirect

Dyes and Pigments

journal homepage: www.elsevier.com/locate/dyepig

A series of highly sensitive and selective fluorescent and colorimetric "off-on" chemosensors for Cu (II) based on rhodamine derivatives

Ming Dong, Tian-Hua Ma, Ai-Jiang Zhang, Yu-Man Dong, Ya-Wen Wang*, Yu Peng*

Key Laboratory of Nonferrous Metal Chemistry and Resources Utilization of Gansu Province, State Key Laboratory of Applied Organic Chemistry and College of Chemistry and Chemical Engineering, Lanzhou University, Lanzhou 730000, China

ARTICLE INFO

Article history:
Received 6 February 2010
Received in revised form
11 March 2010
Accepted 16 March 2010
Available online 21 March 2010

Keywords:
Copper ion
Rhodamine
Fluorescent
UV–visible
Naked-eye
Structure–activity relationship

ABSTRACT

Several rhodamine-B (C.I. Basic Violet 10) hydrazide derivatives were employed as specific fluorescent and colorimetric chemosensors for Cu^{2+} in neutral buffered media. The probes exhibited selective "off-on" type changes in both absorption and emission spectra toward Cu^{2+} ions compared to other metal cations, which was attributed to transformation of the non-fluorescent and colorless spirolactam derivative to the ring-opened, fluorescent, pink coloured amide. Further studies of structure-activity relationship revealed that the designated acyl hydrazone skeleton moiety shared by these chemosensors, derived from the dye hydrazide and salicylaldehyde analogues, determines the selectivity for Cu^{2+} over other cations.

1. Introduction

Copper plays an important role in various biological processes because of its ability to cycle between multiple oxidation states [1–3]. However, this redox reactivity is potentially harmful to living organisms, since compromises in homeostatic control of copper pools can result in oxidative stress and subsequent damage to tissue and organ systems [4–6]. Hence the U.S. Environmental Protection Agency (EPA) has established the limit of copper in drinking water at 1.3 ppm (*ca.* 20 μM). In addition, the average concentration of copper in blood is limited to 100–150 μg/dL (15.7–23.6 μM) [7].

Fluorescent chemosensors have served as useful tools for the detection of metal ions owing to their intrinsic sensitivity, selectivity and capacity for rapid, real-time monitoring [8–10]. Since Czarnik and co-workers pioneeringly developed a fluorescent chemodosimeter for Cu^{2+} utilizing rhodamine-B hydrazide in 1997 [11], several such rhodamine-modified, fluorescent chemosensors or chemodosimeters, which are driven by visible light excitation and which display "turn-on" response to targeted metal cations, have been developed [12]. Whereas rhodamine derivatives with a spirolactam-ring are non-fluorescent and colorless, the presence of a metal cation, such as Cr^{6+} [13], Cr^{3+} [14,15], Fe^{3+} [16–20], Cu^{2+} [21–25], Hg^{2+} [26–39], Pb^{2+} [40], Cd^{2+} [41], Ag^{+} [42,43], can result in spirocyclic-opening *via* coordination or irreversible chemical reaction, which accompanied by the appearance of a pink color and orange fluorescence. Although several fluorescent chemosensors have been reported, detailed studies of the structure of the sensors and their functionality are scarce; this stimulated an interest in the preparation of the sensors **RB**, **RN** and **RS** so as to investigate structure-activity relationships (SAR). All such sensors display reversible, selective and sensitive fluorescence enhancement response to Cu^{2+} ions in neutral, buffered media and systematic studies revealed that the designated acyl hydrazone skeleton structure shared by these chemosensors is responsible for the selectivity for Cu^{2+} over other cations.

2. Experimental

2.1. General

Rhodamine-B (C.I. Basic Violet 10; $C_{28}H_{31}N_2O_3 \cdot Cl$, purity: 99%+) and each of the perchlorate salts were obtained from Acros, New Jersey, US. All solutions were prepared in deionised water. Unless otherwise noted, materials were obtained from commercial suppliers and were used without further purification. Flash

* Corresponding authors. Tel.: +86 931 8912552; fax: +86 931 8912582.
E-mail addresses: ywwang@lzu.edu.cn (Y.-W. Wang), pengyu@lzu.edu.cn (Y. Peng).

0143-7208/$ – see front matter Crown Copyright © 2010 Published by Elsevier Ltd. All rights reserved.
doi:10.1016/j.dyepig.2010.03.015

chromatography was carried out using 200–300 mesh silica gel. ^{1}H and ^{13}C NMR spectra were recorded in $CDCl_3$ solution using a Bruker 400 MHz instrument and spectral data are reported in *ppm* relative to tetramethylsilane (TMS) as internal standard. Mass spectra were obtained using a Bruker Daltonics esquire 6000 mass spectrometer. UV–vis absorption spectra were secured using a Varian UV-Cary100 spectrophotometer and fluorescence emission spectra were recorded on a Hitachi F-4500 fluorescence spectrofluorometer. pH was measured using a Sartorius PB-10 pH meter equipped with a PY-ASI combination glass pH electrode.

Stock solutions (10 mM) of the perchlorate salts of Cu^{2+}, Hg^{2+}, Zn^{2+}, Mg^{2+}, Pb^{2+}, Cd^{2+}, Ag^{+}, Fe^{2+}, Fe^{3+}, Mn^{2+}, Co^{2+}, Ni^{2+}, Li^{+}, Na^{+}, K^{+}, Mg^{2+}, Ca^{2+}, and Ba^{2+} in water were prepared. Stock solutions of the host compounds (1 mM) were prepared in CH_3CN–HEPES (0.01 M, pH = 7.04) (2:8 v/v). Test solutions were prepared by placing 10 μL of the probe stock solution in a test tube, adding an appropriate aliquot of each stock metal salt and diluting the resulting solution to 2 mL with CH_3CN–HEPES (0.01 M, pH = 7.04) (2:8 v/v). For all measurements, fluorescence spectra were obtained by excitation of the rhodamine fluorophore at 530 nm; both the excitation and emission slit widths were 5 nm.

2.2. Synthesis

2.2.1. Synthesis of *RB*, *RN*, and *RS*

The synthesis of the rhodamine–binaphthol derivative **RB**, rhodamine–naphthalene derivative **RN** and the rhodamine–salicylaldehyde derivative **RS** is shown in Scheme 1. Starting from 1, 1′-bi-2-naphthol (BINOL), compounds (*R*)-**2**, (*R*)-**3** and (*R*)-**4** were synthesized according to the literature [44]. **1** was synthesized by modifying the reported procedure [45] with an improved yield of 90%. **1** was then reacted with the (*R*)-BIONL derivative (*R*)-**4** to give **RB** in 93% yield. The reaction of **1** with 2-hydroxy-1-naphthaldehyde or 2-methoxy-benzaldehyde in refluxing ethanol afforded **RN** in 93% yield or **RS** in 82% yield.

2.2.2. Rhodamine-B hydrazide (*1*)

A stirred solution of Rhodamine-B (0.48 g, 1 mmol), and hydrazine hydrate (85%, 0.28 mL, 5 mmol) in EtOH (30 mL) was refluxed for 10 h. After cooling to room temperature, the solvent was evaporated under vacuum and the resulting solid was diluted with CH_2Cl_2 (50 mL) and washed with H_2O (3 × 50 mL) followed by drying over anhydrous Na_2SO_4. After filtration of sodium sulfate, removal of the solvent *in vacuo* gave 0.41 g of **1** (90%) as a yellow solid. ^{1}H NMR ($CDCl_3$, 400 MHz): δ 1.16 (t, J = 7.0 Hz, 12H), 3.34 (q, J = 7.0 Hz, 8H), 3.61 (s, 2H), 6.27 (d, J = 2.8 Hz, 1H), 6.30 (d, J = 2.4 Hz, 1H), 6.42 (d, J = 2.4 Hz, 2H), 6.45 (s, 1H), 6.47 (s, 1H), 7.10 (m, 1H), 7.44 (m, 2H), 7.94 (m, 1H) ppm; ^{13}C NMR ($CDCl_3$, 100 Hz): δ 11.9, 43.7, 65.3, 96.4, 103.6, 107.5, 122.7, 123.2, 127.6, 128.4, 131.8, 147.4, 150.9, 153.6, 165.3 ppm; ESI–MS: (m/z) 457.3 $[M+H]^+$.

2.2.3. (*R*)-2,2′-bis(methoxymethyloxy)-1,1′-binaphthalene ((*R*)-*2*)

NaH (1.92 g, 80 mmol) was added to DMF (30 mL) in an ice bath. (*R*)-BINOL ((*R*)-2, 2′-dihydroxy-1,1′-binaphthyl) (10 g, 34 mmol) in DMF (50 mL) was added dropwise to this solution over 20 min. After a further 30 min, MOMCl (chloromethyl methyl ether) (6.4 g, 80 mmol) was added dropwise to the above solution over 20 min. The reaction was monitored by TLC. After stirring for 1 h, the reaction mixture was quenched with water and extracted with chloroform (2 × 100 mL). The crude product was purified by flash chromatography (Pet/EtOAc = 5:1) on silica gel (95 % yield). ^{1}H NMR ($CDCl_3$, 400 MHz): δ 3.15 (s, 6H), 4.99 (d, J = 6.6 Hz, 2H), 5.05 (d, J = 6.6 Hz, 2H), 7.12–7.37 (m, 6H), 7.56 (d, J = 9.0 Hz, 2H), 7.87 (d, J = 8.1 Hz, 2H), 7.94 (d, J = 9.0 Hz, 2H) ppm; ^{13}C NMR ($CDCl_3$, 100 MHz): δ 55.8, 95.1, 117.2, 121.2, 124.0, 125.5, 126.2, 127.8, 129.4, 129.8, 134.0, 152.6 ppm; ESI-MS: (m/z) 375.1 $[M+H]^+$.

2.2.4. (*R*)-3-formyl-2,2′-bis(methoxymethyloxy)-1,1′-binaphthalene ((*R*)-*3*)

To a stirred solution of (*R*)-**2** (3.2 g, 8.55 mmol) in THF (30 mL) at −78 °C was added TMEDA (1.55 mL, 10.3 mmol) and then *n*-BuLi (6.08 mL, 9.67 mmol, 1.6 M in hexane) was added over 15 min. The

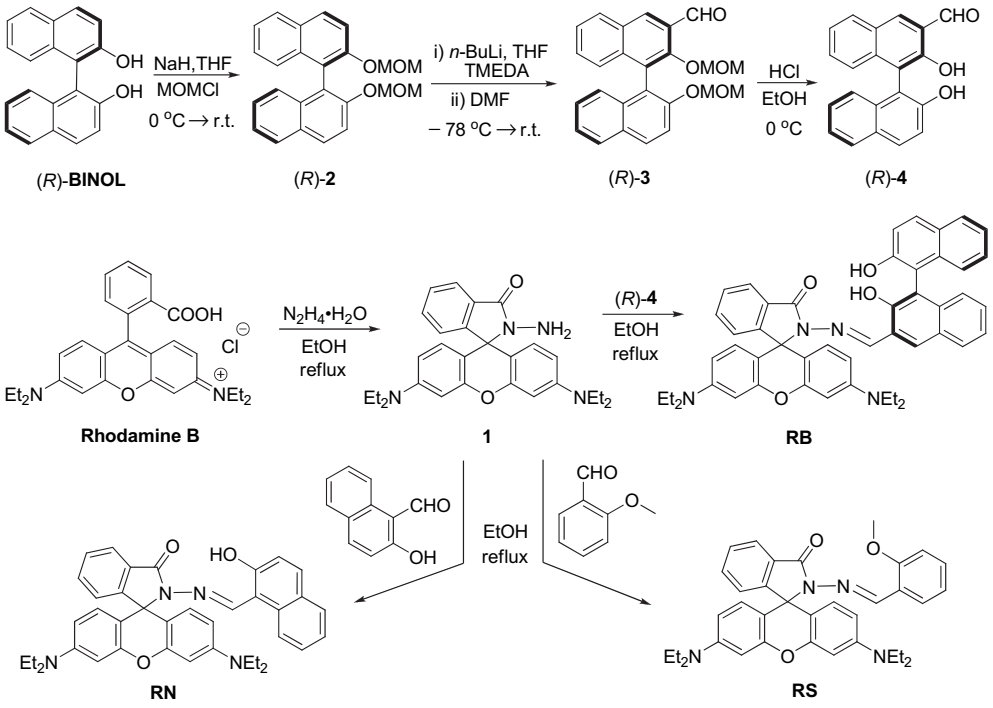

Scheme 1. The synthesis of compounds **RB**, **RN**, and **RS**.

mixture was warmed to 0 °C and stirred for 30 min. After cooling to −78 °C, DMF (0.76 mL, 10.3 mmol) in THF (40 mL) was added dropwise over 10 min. The mixture was stirred at −78 °C for 30 min and then was warmed to 0 °C and stirred for a further 40 min. The resulting yellow solution was quenched with saturated NH_4Cl (5 mL). After the addition of 1 M aq HCl (5 mL), the solution was extracted with diethyl ether (100 mL), and the combined organic layers were washed with saturated $NaHCO_3$ (50 mL) and brine and then dried over $MgSO_4$. The solvent was evaporated under reduced pressure and the crude product was purified by flash chromatography (Pet/EtOAc = 15:1) on silica gel to give 2.4 g of (*R*)-**3** (70%). ^{1}H NMR ($CDCl_3$, 400 MHz): δ 3.07 (s, 3H), 3.20 (s, 3H), 4.64 (d, J = 6.1 Hz, 1H), 4.74 (d, J = 6.1 Hz, 1H), 5.03 (d, J = 7.3 Hz, 1H), 5.21 (d, J = 7.3 Hz, 1H), 7.16–7.64 (m, 7H), 7.82–8.17 (m, 3H), 8.61 (s, 1H), 10.63 (s, 1H) ppm; ^{13}C NMR ($CDCl_3$, 100 MHz): δ 56.0, 57.1, 94.5, 100.2, 116.3, 119.4, 124.3, 125.2, 125.9, 126.0, 126.8, 126.9, 128.0, 129.0, 129.6, 130.1, 130.2, 130.3, 131.0, 133.7, 137.0, 152.8, 153.8, 191.2 ppm; ESI − MS: (*m/z*) 403.1 $[M + H]^+$.

2.2.5. *(R)-2,2′-dihydroxy-1,1′-binaphthyl-3-carbaldehyde ((R)-**4**)*

To an ice-cooled solution of (*R*)-**3** (5.15 g, 12.8 mmol) in EtOH (80 mL) was added (6 N) HCl (30 mL) and the ensuing mixture was stirred for 3 h at 0 °C. The mixture was extracted with ethyl ether (3 × 100 mL) and the combined organic extracts were washed with brine, dried over $MgSO_4$ and evaporated under reduced pressure. The residue was then dried *in vacuo* to afford (*R*)-**4** which was directly used for the next step without purification (95% yield). ^{1}H NMR ($CDCl_3$, 400 MHz): δ 5.01 (s, 1H), 7.06–7.44 (m, 7H), 7.85–7.99 (m, 3H), 8.33 (s, 1H), 10.13 (s, 1H), 10.60 (s, 1H) ppm; ^{13}C NMR ($CDCl_3$, 100 MHz): δ 76.7, 77.0, 77.3, 113.2,115.1, 117.7, 122.1, 123.5, 124.4, 124.9, 125.0, 126.7, 127.8, 128.3, 129.2, 130.0, 130.4, 131.2, 133.4, 137.6, 139.1, 151.4, 154.3, 196.6 ppm; ESI-MS: (*m/z*) 315.1 $[M + H]^+$.

2.2.6. *Compounds of **RB**, **RN** and **RS***

A stirred solution of **1** (0.456 g, 1 mmol), aldehyde (0.314 g, 1 mmol) ((*R*)-**4** or 2-hydroxy-1-naphthaldehyde or 2-methoxybenzaldehyde) in EtOH (50 mL) was heated under reflux for 6 h under N_2 in the dark. After the ethanol had been evaporated under reduced pressure, the residue was purified by silica gel column chromatography (CH_2Cl_2/MeOH/Et_3N = 200:1:1) to give **RB** (93%) or **RN** (93%) or **RS** (82%).

RB: ^{1}H NMR ($CDCl_3$, 400 MHz): δ 1.08 (t, J = 6.8 Hz, 6H), 1.16 (t, J = 6.8 Hz, 6H), 3.27 (q, J = 6.8 Hz, 4H), 3.33 (q, J = 6.8 Hz, 4H), 5.09 (s, 1H), 6.27 (m, 2H), 6.39 (d, J = 2.8 Hz, 1H), 6.44 (d, J = 2.4 Hz, 1H), 6.53 (m, 2H), 7.02 (s, 2H), 7.14 (d, J = 6.8 Hz, 2H), 7.19 (m, 2H), 7.28 (s, 1H), 7.33 (d, J = 8.4 Hz, 1H), 7.51 (m, 2H), 7.75 (s, 1H), 7.79 (d, J = 8.0 Hz, 1H), 7.84 (d, J = 8.0 Hz, 1H), 7.88 (d, J = 8.8 Hz, 1H), 7.99 (d, J = 6.8 Hz, 1H), 8.96 (s, 1H), 11.12 (s, 1H) ppm; ^{13}C NMR ($CDCl_3$, 100 MHz): δ 12.5, 44.2, 65.8, 97.9, 104.8, 108.0, 114.8, 115.2, 118.3, 120.9, 122.8, 123.6, 124.9, 126.0, 128.0, 128.4, 129.0, 129.4, 129.9, 132.4, 133.4, 133.7, 134.7, 138.9, 149.0, 150.2, 151.5, 151.6, 152.0, 153.0, 153.5, 153.8 ppm; ESI-MS: (*m/z*) 753.2 $[M + H]^+$.

RN: ^{1}H NMR ($CDCl_3$, 400 MHz): δ 1.14 (t, J = 6.8 Hz, 12H), 3.31 (q, J = 6.8 Hz, 8H), 5.30 (s, 1H), 6.26 (d, J = 2.4 Hz, 2H), 6.28 (d, J = 2.4 Hz, 2H), 6.53 (m, 2H), 7.10 (d, J = 8.8 Hz, 1H), 7.20 (d, J = 7.2 Hz, 1H), 7.29 (d, J = 7.8 Hz, 1H), 7.44 (t, J = 8.8 Hz, 1H), 7.54 (t, J = 5.2 Hz, 2H), 7.67 (m, 2H), 7.85 (d, J = 8.8 Hz, 1H), 8.03 (d, J = 6.4 Hz, 1H), 9.86 (s, 1H), 12.24 (s, 1H) ppm; ^{13}C NMR ($CDCl_3$, 100 MHz): δ 12.5, 44.3, 66.3, 97.8, 105.0, 108.2, 109.0, 119.4, 120.4,

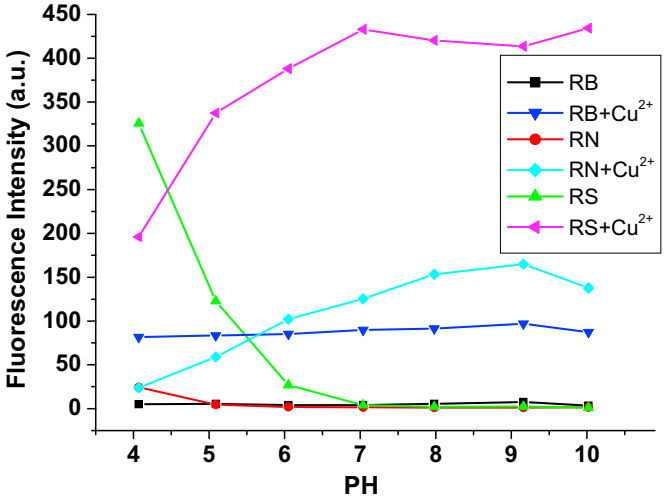

Fig. 1. Fluorescence intensity of **RB**, **RN** and **RS** (5 μM) in CH_3CN–HEPES (0.01 M, pH = 7.04) (2:8 v/v) of different pH in the absence (square, at 561 nm) and presence (triangle at 571 nm) of 25 μM Cu^{2+}.

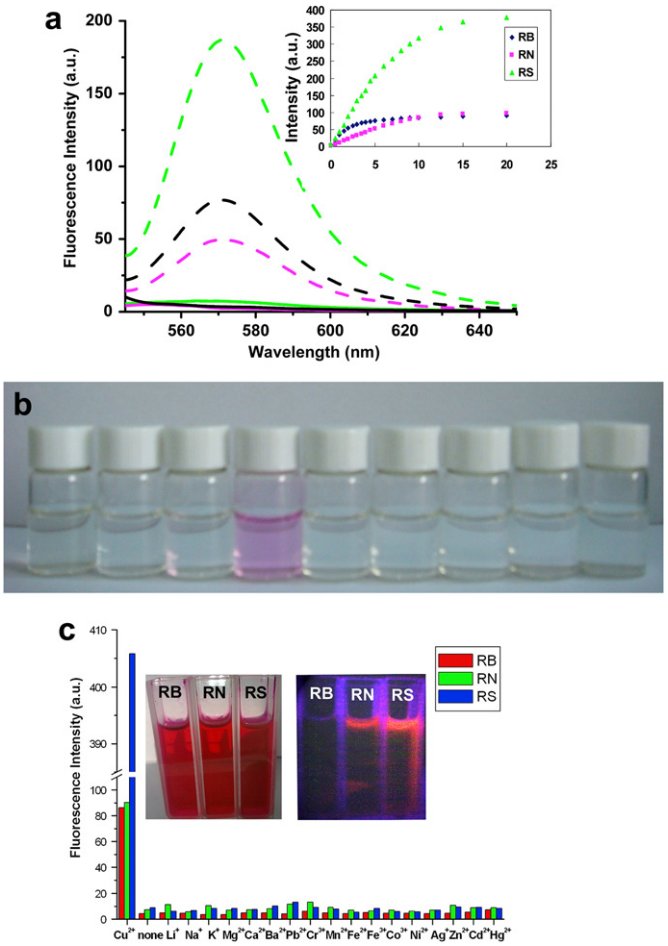

Fig. 2. (a) Fluorescent spectra of **RB**, **RN** and **RS** in the presence of 5 μM Cu^{2+} in CH_3CN–HEPES buffer (0.01 M, pH = 7.04) (2:8, v/v). [**RB**] = [**RN**] = [**RS**] = 5 μM. Excitation wavelength was 530 nm. Inset: Fluorescence intensity at 571 nm as a function of Cu^{2+} concentration; (b) **RB** (50 μM) as a selective naked-eye chemosensor for Cu^{2+} in CH_3CN–HEPES buffer (0.01 M, pH =7.04) (2:8, v/v). From left to right: 100 μM Fe^{3+}, Co^{2+}, Ni^{2+}, Cu^{2+}, Ag^+, Zn^{2+}, Cd^{2+}, Hg^{2+} and Pb^{2+}; (c) Fluorescence responses of **RB**, **RN** and **RS** (5 μM) to various cations (25 μM) at 571 nm in CH_3CN–HEPES buffer (0.01 M, pH = 7.04) (2:8, v/v). Inset: Pictures of **RB**, **RN** and **RS** as a selective naked-eye chemosensors (left) and the visual fluorescence emissions by using a UV lamp (365 nm) (right) for Cu^{2+}.

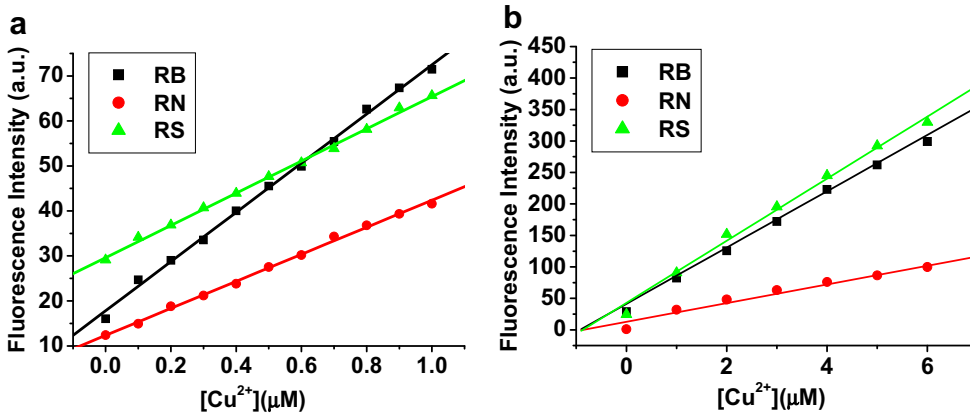

Fig. 3. Fluorescence intensity changes of **RB**, **RN** and **RS** (10 μM) with respect to Cu^{2+} in the concentration range of (a) 6.35–63.5 ppb (0.1–1.0 μM), and (b) 0.064–0.381 ppm (1.0–6.0 μM) in CH_3CN–HEPES buffer (0.01 M, pH = 7.04) (2:8, v/v). The intensity was taken as the peak height at 571 nm. (1.0 μM of Cu^{2+} in the form of $Cu(ClO_4)_2$ is equal to 0.0635 ppm of Cu^{2+}).

123.1, 123.3, 124.1, 127.1, 127.9, 128.1, 128.3, 128.6, 128.7, 129.7, 132.4, 133.5, 148.0, 149.1, 151.2, 153.4, 158.8, 164.1 ppm; ESI – MS: (*m/z*) 611.2 $[M + H]^+$.

RS: ^1H NMR ($CDCl_3$, 400 MHz): δ 1.14 (t, $J = 6.8$ Hz, 12H), 3.33 (q, $J = 6.8$ Hz, 8H), 5.30 (s, 1H), 6.23 (d, $J = 8.4$ Hz, 2H), 6.29 (m, 1H), 6.46 (d, $J = 8.8$ Hz, 1H), 6.52 (d, $J = 8.8$ Hz, 2H), 6.74 (d, $J = 8.4$ Hz, 1H), 6.86 (t, $J = 7.8$ Hz, 1H), 7.11 (d, $J = 7.2$ Hz, 1H), 7.21 (t, $J = 8.0$ Hz, 1H), 7.46 (t, $J = 3.2$ Hz, 2H), 7.58 (d, $J = 6.0$ Hz, 1H), 7.99 (m, 1H), 9.06 (s, 1H) ppm; ^{13}C NMR ($CDCl_3$, 100 MHz): δ 12.6, 44.3, 65.8, 97.8, 97.9, 104.5, 106.0, 107.9, 108.0, 110.6, 111.1, 120.6, 123.0, 123.2, 123.8, 124.1, 126.2, 127.2, 128.1, 129.4, 130.0, 130.7, 132.5, 133.1, 143.6, 148.8, 151.3, 152.0, 153.1, 153.8, 158.2, 164.8,166.1 ppm; ESI – MS: (*m/z*) 585.4 $[M + H]^+$.

The above **RB**, **RN** and **RS** compounds were designed to chelate with metal ions *via* the carbonyl *O*, imino *N* and the phenol *O* groups [46]. The spirolactam moiety of the rhodamine group acted as a signal switcher, which was envisioned to turn on when the cation was bound to the sensor. In the ^{13}C NMR spectrum, the characteristic peak of the spirolactam quaternary C at or near 66 ppm indicated that the spirolactam form existed predominantly [47].

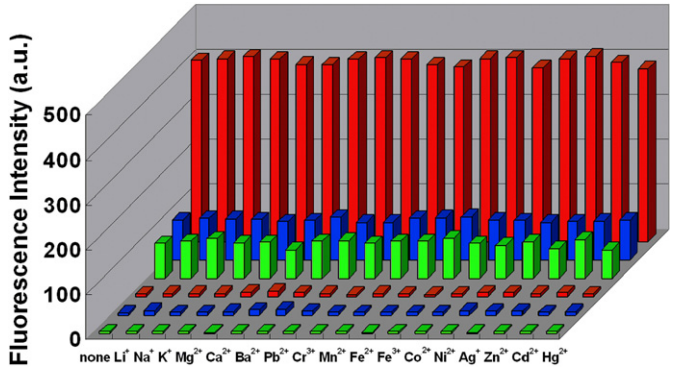

Fig. 4. Fluorescence responses of **RB** (green bars), **RN** (blue bars) and **RS** (red bars) (5 μM) to various cations in CH_3CN–HEPES buffer (0.01 M, pH = 7.04) (2:8, v/v). The front three bars represent the emission intensities of **RB**, **RN** and **RS** in the presence of other cations (50 μM), respectively. The back three bars represent the emission intensities that occur upon the subsequent addition of 5 μM of Cu^{2+} to the above solution, respectively. The emission intensities were recorded at 571 nm, and the excitation wavelength was 530 nm. (For interpretation of the references to colour in this figure legend, the reader is referred to the web version of this article.)

2.3. Determination of binding constants [48]

Assuming a 1: *n* stoichiometry for interaction between L and Cu^{2+}, the equilibrium is given by the following equation:

$$L + nCu^{2+} \overset{K}{\rightleftharpoons} LCu_n^{2+} \tag{2}$$

The association constant, *K*, is therefore expressed as:

$$K = \frac{\left[LCu_n^{2+}\right]}{[L]\left[Cu^{2+}\right]^n} = \frac{\left[LCu_n^{2+}\right]}{\left([L]_0 - \left[LCu_n^{2+}\right]\right)\left(\left[Cu^{2+}\right]_0 - n\left[LCu_n^{2+}\right]\right)^n} \tag{3}$$

$[LCu^{2+}{}_n]$, [L], and $[Cu^{2+}]$ represent the equilibrium concentrations of the complex, free L, and free Cu^{2+}, respectively. $[L]_0$ and $[Cu^{2+}]_0$ are the initial concentrations of L and Cu^{2+}, respectively. If $[Cu^{2+}]_0 \gg [LCu^{2+}{}_n]$, the Eq. (3) can be simplified as follows:

$$K = \frac{\left[LCu_n^{2+}\right]}{\left([L]_0 - \left[LCu_n^{2+}\right]\right)\left(\left[Cu^{2+}\right]_0\right)^n} \tag{4}$$

Then it can be transformed to:

$$K\left[Cu^{2+}\right]_0^n = \frac{\left[LCu_n^{2+}\right]}{[L]_0 - \left[LCu_n^{2+}\right]} \tag{5}$$

Fluorescence intensity is given by following equations:

$$\frac{F - F_{min}}{F_{max} - F} = \frac{\left[LCu_n^{2+}\right]}{\left[LCu_n^{2+}\right]_{max} - \left[LCu_n^{2+}\right]} = \frac{\left[LCu_n^{2+}\right]}{[L]_0 - \left[LCu_n^{2+}\right]} \tag{6}$$

F_{min} is the fluorescence intensity of L without cations, *F* is the fluorescence intensity of L obtained with Cu^{2+}, F_{max} is the fluorescence intensity of L in the presence of excess amount of Cu^{2+}. In the presence of excess amount of Cu^{2+}, $[LCu^{2+}{}_n]_{max}$ is almost equal to $[L]_0$. Using Eqs. (5) and (6), the following equation is given:

$$\frac{F - F_{min}}{F_{max} - F} = K\left[Cu^{2+}\right]_0^n \tag{7}$$

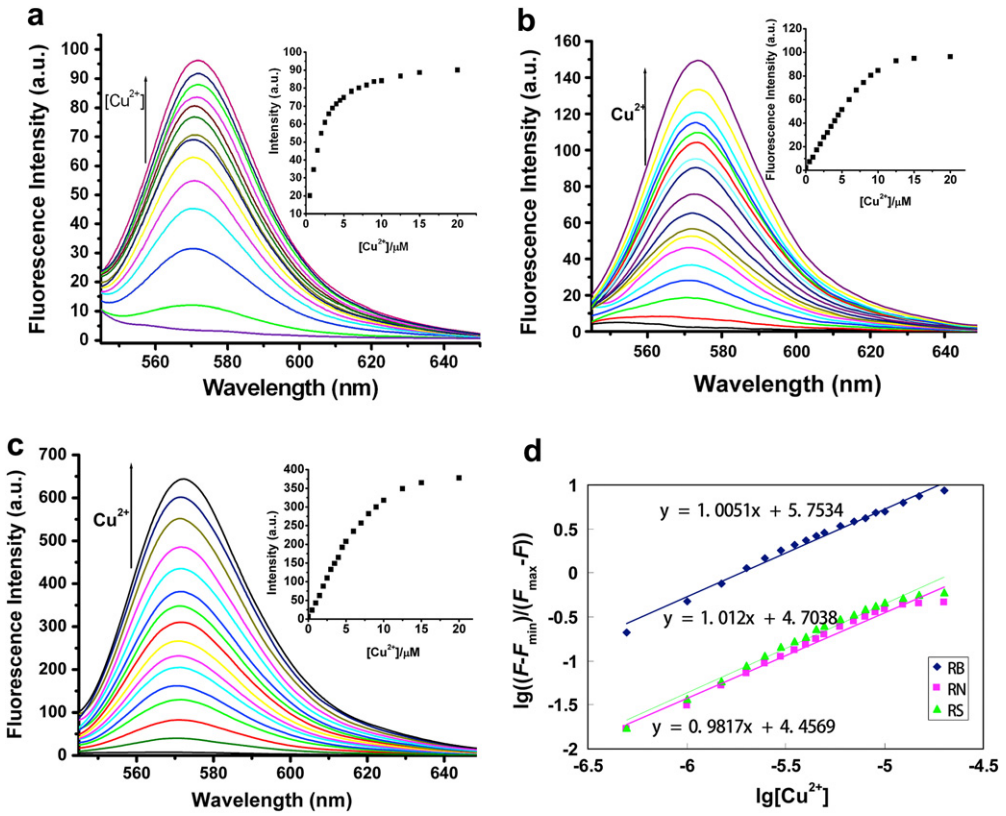

Fig. 5. Fluorescent spectra of (a) **RB**, (b) **RN** and (c) **RS** in the presence of different concentrations of Cu^{2+} in CH_3CN–HEPES buffer (0.01 M, pH = 7.04) (2:8, v/v). Excitation wavelength was 530 nm. Inset: fluorescence intensity at 571 nm as a function of Cu^{2+} concentration; (d) The nonlinear fitting (fluorescent emission at 571 nm) of **RB**, **RN** or **RS**lg $[(F - F_{min})/(F_{max} - F)] = \lg K + \lg[Cu^{2+}]$. K is the association constant, F_{min} is the fluorescence intensity of **RB**, **RN** or **RS** without any cations, F is the fluorescence intensity of **RB**, **RN** or **RS** obtained with Cu^{2+}, F_{max} is the fluorescence intensity of **RB**, **RN** or **RS** in the presence of excess amount of Cu^{2+}.

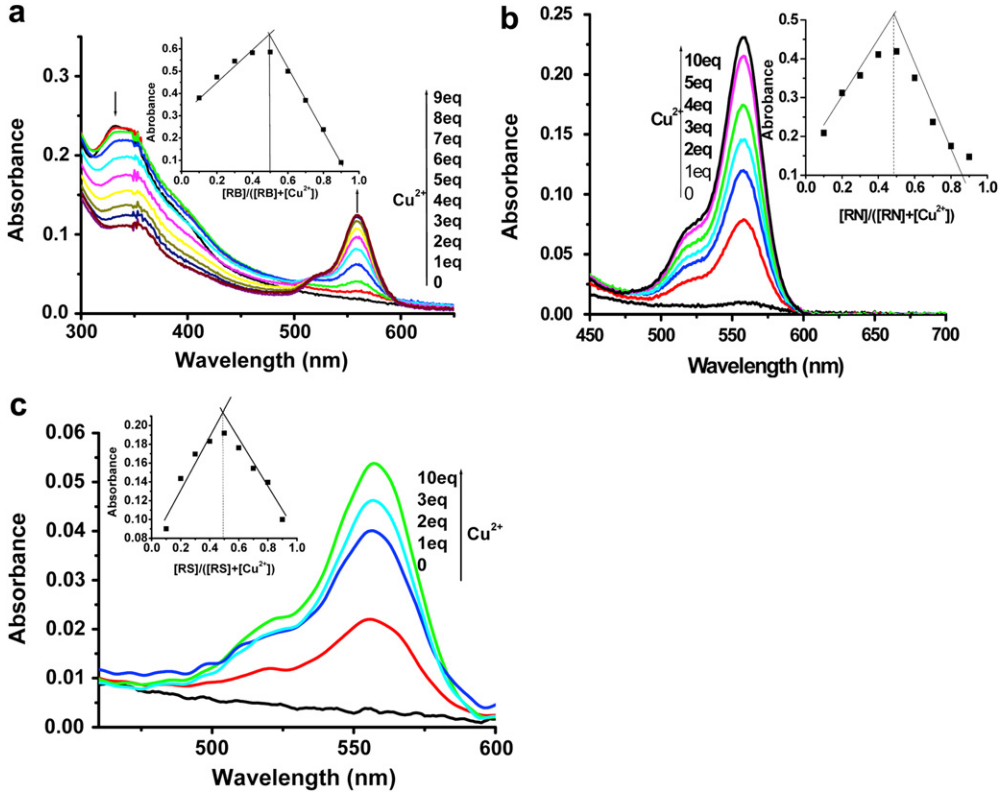

Fig. 6. Absorption spectra of (a) **RB**, (b) **RN** and (c) **RS** (5 μM) in the presence of different concentrations of Cu^{2+} in CH_3CN–HEPES buffer (0.01 M, pH = 7.04) (2:8, v/v). Inset: Job's plots at 555 nm (**RB**, **RN** and **RS**).

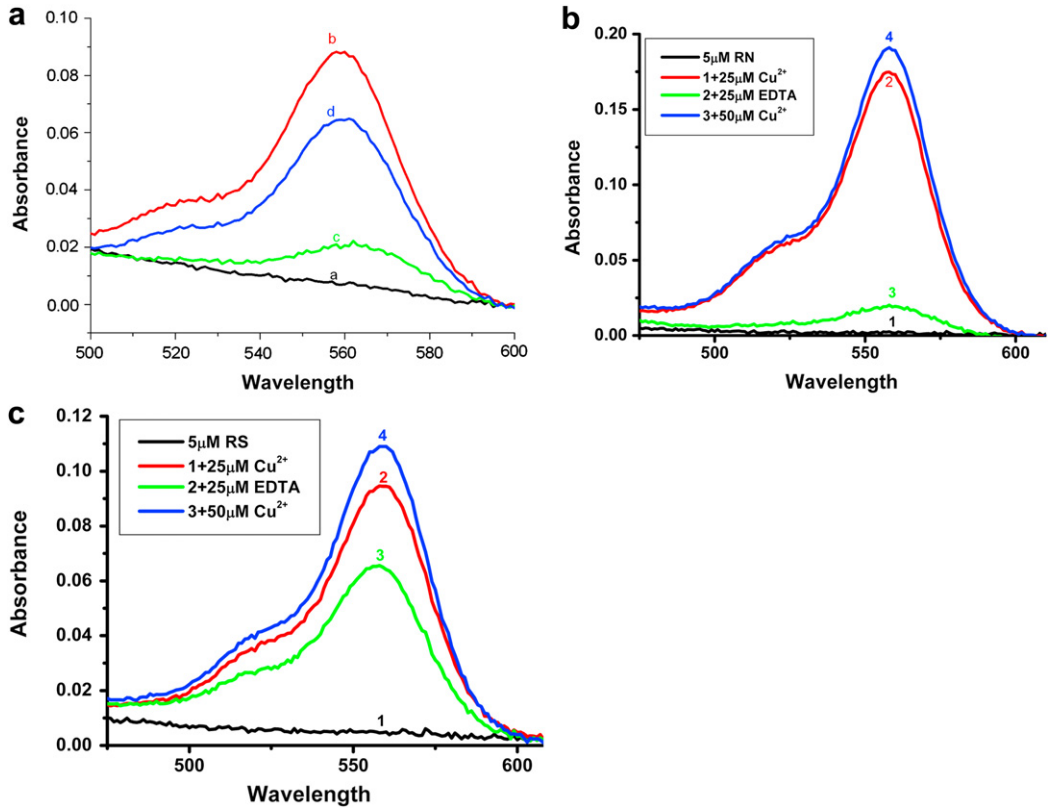

Fig. 7. Reversible titration responses of (a) **RB**, (b) **RN** and (c) **RS** to Cu^{2+} in CH_3CN–HEPES buffer (0.01 M, pH = 7.04) (2:8, v/v): (1) 5 μM **RB** (**RN** or **RS**); (2) 5 μM **RB** (**RN** or **RS**) with 25 μM Cu^{2+}; (3) 5 μM **RB** (**RN** or **RS**) with 25 μM Cu^{2+} and then addition of 25 μM EDTA (sodium salt); (4) 5 μM **RB** (**RN** or **RS**) with 25 μM Cu^{2+}, 25 μM EDTA and then addition of 50 μM Cu^{2+}.

$$\lg\frac{F-F_{\min}}{F_{\max}-F} = \lg K + n\lg[Cu^{2+}]_0 \quad (8)$$

When assuming the 1:1 stoichiometry ($n = 1$), Eq. (1) is obtained.

$$\lg\frac{F-F_{\min}}{F_{\max}-F} = \lg K + \lg[Cu^{2+}] \quad (1)$$

3. Results and discussion

3.1. Detection range of pH value

The pH dependence of the fluorescence intensity of **RB**, **RN**, **RS** and **RB**–Cu^{2+}, **RN**–Cu^{2+}, **RS**–Cu^{2+} system was shown in Fig. 1. The response reached a maximum value and remained a constant between pH 4.0 and 10.0, 5.0 and 10.0, 7.0 and 10.0, respectively. Especially, either free ligand or complex of **RB**, were the most insensitive against H^+ or OH^-. In subsequent experiments, a CH_3CN–HEPES buffer solution (pH = 7.0) was used as an ideal experimental media.

3.2. Complexation studies of *RB*, *RN* and *RS* with Cu^{2+}

Fluorescence spectra of **RB**, **RN** and **RS** were measured by the addition of 1.0 equiv of Cu^{2+} in CH_3CN–HEPES buffer (0.01 M, pH = 7.04) (2:8, v/v) (Fig. 2a). The free **RB**, **RN** and **RS** did not exhibit apparent emission band above 500 nm and remained colorless, which indicated that the spirolactam form was the predominant species at that time. A new strong fluorescence emission band

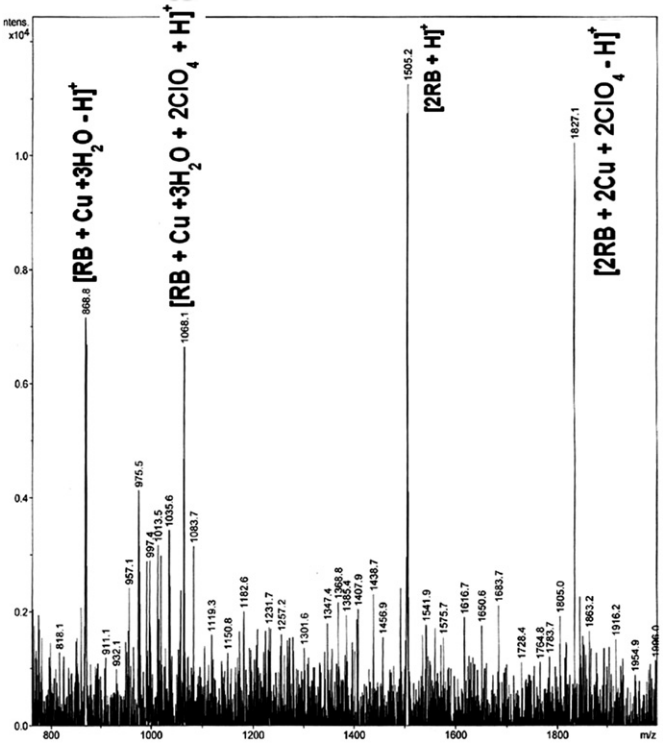

Fig. 8. ESI mass spectrum of **RB** in the presence of 3.0 equiv of Cu^{2+}.

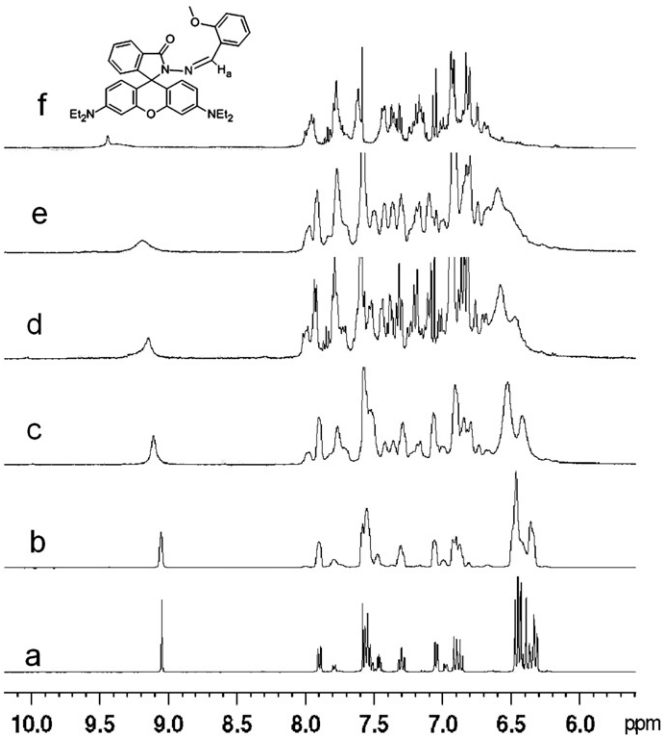

Fig. 9. Partial ^{1}H NMR spectra of **RS** (25 mM) with Cu^{2+} in CD_3CN. (a) **RS** only; (b) **RS** + 0.2 equiv of $Cu(ClO_4)_2$; (c) **RS** + 0.4 equiv of $Cu(ClO_4)_2$; (d) **RS** + 0.6 equiv of $Cu(ClO_4)_2$; (e) **RS** + 0.8 equiv of $Cu(ClO_4)_2$; (f) **RS** + 1.0 equiv of $Cu(ClO_4)_2$.

centered at 571 nm was observed, and a simultaneous color change was also found (from colorless to pink) upon the addition of Cu^{2+}, which was attributed to the Cu^{2+} induced ring-opening of the spirolactam moiety. After the addition of the respective metal ions including Li^+, Na^+, K^+, Mg^{2+}, Ca^{2+}, Ba^{2+}, Pb^{2+}, Cr^{3+}, Mn^{2+}, Fe^{2+}, Fe^{3+}, Co^{2+}, Ni^{2+}, Ag^+, Zn^{2+}, Cd^{2+} and Hg^{2+}, the fluorescence intensity at 571 nm was not induce any apparent fluorescent enhancement and no color change (compared to that in the presence of Cu^{2+}) (Fig. 2b and c), which clearly indicated that **RB**, **RN** and **RS** could be used as potential fluorescent chemosensors for Cu^{2+}. But when 5.0 equiv of Cu^{2+} was added to the different ligand solutions, different increase of fluorescence intensities at 571 nm were observed, where almost 22-fold enhancement of I/I_0 for **RB**, 21-fold for **RN**, and 30-fold for **RS**, respectively. (Herein, I_0 indicates the fluorescence intensity of free **RB**, **RN** or **RS**, while I indicates the fluorescence intensity of corresponding complexes upon the addition of 5 equiv of Cu^{2+}). These results suggested that the highest emission enhancements were obtained with **RS** receptor in the sensing for Cu^{2+}. The corresponding detection limits [42] of **RB**, **RN** and **RS** toward Cu^{2+} are all 0.20 μM (12.7 ppb) by plotting the fluorescence intensity at 571 nm versus the concentration of Cu^{2+} (Fig. 3).

To validate the selectivity of **RB**, **RN** or **RS** in practice, the competition experiments were also measured by addition of 1.0 equiv of Cu^{2+} to their aqueous solutions in the presence of 10.0 equiv of other metal ions and shown in Fig. 4. The selectivity of **RB**, **RN** or **RS** to Cu^{2+} was still satisfactory. All competitive metal ions had no obvious interference with the detection of Cu^{2+} ion, which indicated that the system of **RB**–Cu^{2+}, **RN**–Cu^{2+} or **RS**–Cu^{2+} was hardly affected by these coexistent ions.

The fluorescent titration experiments (Fig. 5a, b and c) displayed the fluorescence turn-on response of **RB**, **RN** or **RS** to Cu^{2+} ions. The nonlinear fitting of the titration curve (Fig. 5d) confirmed a 1:1 stoichiometry between **RB**, **RN** or **RS** and Cu^{2+} with the association constants of $5.6 \times 10^5\ M^{-1}$, $5.0 \times 10^4\ M^{-1}$ and $3.7 \times 10^4\ M^{-1}$ respectively, which suggested that the complex of **RB**–Cu^{2+} was more stable than that of **RN**–Cu^{2+} and **RS**–Cu^{2+}.

The UV–vis absorption spectra of **RB**, **RN** and **RS** (Fig. 6) were recorded in CH_3CN–HEPES buffer (0.01 M, pH = 7.04) (2:8, v/v). A new strong absorption band centered at *ca.* 555 nm was observed after addition of Cu^{2+}. The differences of the UV–vis absorption spectra between the system of **RB**–Cu^{2+} and the system of **RN**–Cu^{2+} or **RS**–Cu^{2+} were that the absorption band around 335 nm became weak gradually in the presence of Cu^{2+} and an isosbestic point at 505 nm was observed in the UV–vis absorption spectrum of the system of **RB**–Cu^{2+}, but there was no significant

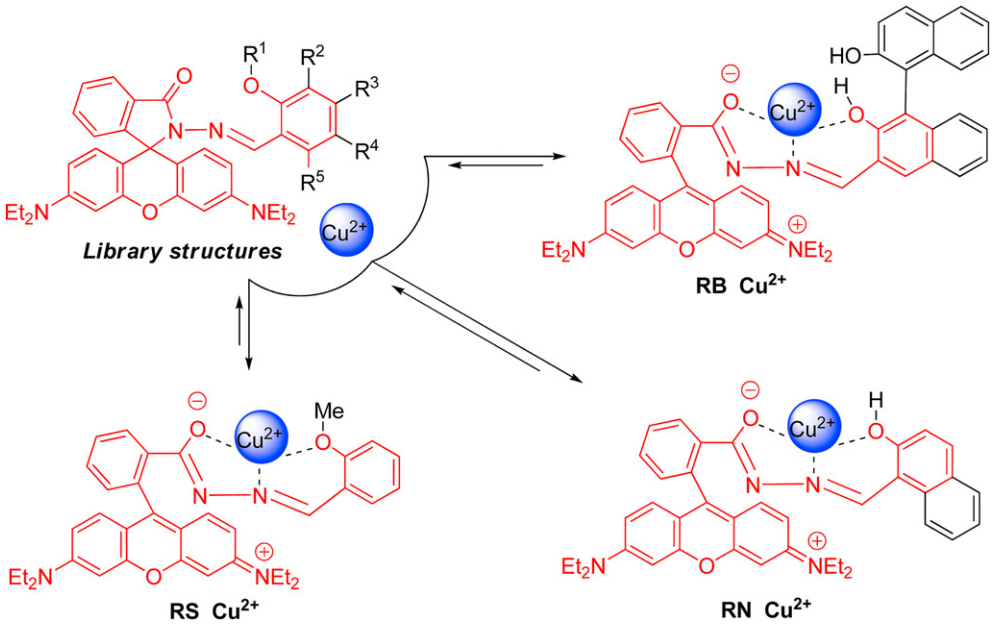

Fig. 10. Proposed binding mode between rhodamine derivatives and Cu^{2+}.

changes at short wavelengths in the UV–vis absorption spectrum of the system of **RN**–Cu^{2+} or **RS**–Cu^{2+}. When Cu^{2+} was added to the different ligand solutions, different increase of absorbance intensities at 555 nm were observed, where almost 4-fold enhancement of A/A_0 for **RB**, 20-fold for **RN**, and 18-fold for **RS**, respectively. (Herein, A_0 indicates the absorbance intensity of free **RB**, **RN** or **RS**, A is the absorbance intensity upon addition of 10.0 equiv of Cu^{2+}). The required equivalences of Cu^{2+} to stabilize the absorbance intensity were 7, 5 and 3, respectively. These results indicated that the enhancements of absorption band were improved as decreasing the rigidity of salicylaldehyde analogues moiety. The Job's plots also indicated a 1:1 stoichiometry between **RB**, **RN** or **RS** and Cu^{2+}. Reversible titration using EDTA/Cu^{2+} (Fig. 7) demonstrated that the above absorption responses were also reversible.

These studies suggested that **RB**, **RN** and **RS** could be served as reversible naked-eye Cu^{2+}-specific fluorescent chemosensors in neutral buffered media.

3.3. The proposed binding mechanism and comparison of *RB*, *RN* and *RS* regarding sensing ability for Cu^{2+}

The photophysical properties revealed that 1:1 complex was formed between **RB**, **RN** or **RS** and Cu^{2+}. More direct evidence was obtained by the ESI mass spectrum of the system of **RB**–Cu^{2+} (Fig. 8). The peaks of $[\mathbf{RB} + Cu + 3H_2O - H]^+$ (calcd = 669.3), $[\mathbf{RB} + Cu + 3H_2O + 2ClO_4 + H]^+$ (calcd = 1068.2) and $[2\mathbf{RB} + 2Cu + 2ClO_4 - H]^+$ (calcd = 1827.4) at m/z = 668.8, 1068.1 and 1827.1 were observed when 3.0 equiv of Cu^{2+} was added to **RB**. The above results indicated a plausible interaction mode of **RB**/Cu^{2+} = 1:1. The ^1H NMR titration experiments of **RS** in CD_3CN (Fig. 9) showed that the H_a (9.06 ppm) and aromatic protons (6.2–8.0 ppm) shifted downfield which originated from the coordination of "*N*" and "*O*" to "Cu^{2+}" and became broader which was due to the decrease of electron density, upon the addition of Cu^{2+} [40].

A plausible interaction mode of three complexes are proposed in Fig. 10, in which Cu^{2+} is coordinated cooperatively with carbonyl *O*, imino *N*, and the *ortho*-phenol *O*. The above results suggested that designated acyl hydrazone skeleton embedded in **Library structures** is the essential binding domain responsible for sensing Cu^{2+} for these rhodamine derivatives, which should be consistent with that reported previously [21–23]. Considering structure-activity of **RB**, **RN** and **RS**, we found that the enhancements of the emission band or absorption band were improved (**RB** < **RN** < **RS**). However, for both ligands and complexes, the sensitivities were also increased against H^+ or OH^- (**RB** < **RN** < **RS**) and association constants of complexes were decreased (**RB** > **RN** > **RS**). These results were due to the decreasing of the rigidity of salicylaldehyde analogues moiety (**RB** > **RN** > **RS**). It is noteworthy that combinatorial construction of libraries of fluorescent probe candidates has been demonstrated to be a very powerful and promising approach with some impressive discoveries of novel fluorescent probes recently [49–56].

4. Conclusion

Three new rhodamine derivatives have been synthesized for the detection of Cu^{2+}. All of the sensors **RB**, **RN** and **RS** displayed highly selective and sensitive fluorescent enhancement and colorimetric change upon the addition of Cu^{2+}. The comparison of their sensing ability revealed that there is intrinsic correlation between the designated acyl hydrazone skeleton structure from these rhodamine-salicylaldehyde analogues (Fig. 8) and the selectivity for Cu^{2+} than other cations.

Acknowledgments

This work was financially supported by the National Natural Science Foundation of China (No. 20802029), and the Fundamental Research Funds for the Central Universities (lzujbky-2009-72).

References

[1] Maryon EB, Molloy SA, Zimnicka AM, Kaplan JH. Copper entry into human cells: progress and unanswered questions. BioMetals 2007;20:355–64.
[2] Leary SC, Winge DR, Cobine PA. "Pulling the plug" on cellular copper: the role of mitochondria in copper export. Biochimica et Biophysica Acta - Molecular Cell Research 2009;1793:146–53.
[3] Turski ML, Thiele DJ. New roles for copper metabolism in cell proliferation, signaling, and disease. The Journal of Biological Chemistry 2009;284:717–21.
[4] Valentine JS, Doucette PA, Potter SZ. Copper-zinc superoxide dismutase and amyotrophic lateral sclerosis. Annual Review of Biochemistry 2005;74:563–93.
[5] Gaggelli E, Kozlowski H, Valensin D, Valensin G. Copper homeostasis and neurodegenerative disorders (Alzheimer's, prion, and Parkinson's diseases and amyotrophic lateral sclerosis). Chemical Reviews 2006;106:1995–2044.
[6] Millhauser GL. Copper and the prion protein: methods, structures, function, and disease. Annual Review of Physical Chemistry 2007;58:299–320.
[7] Jung HS, Kwon PS, Lee JW, Kim JI, Hong CS, Kim JW, et al. Coumarin-derived Cu^{2+}-selective fluorescence sensor: synthesis, mechanisms, and applications in living cells. Journal of the American Chemical Society 2009;131:2008–12.
[8] de Silva AP, Gunaratne HQN, Gunnlaugsson T, Huxley AJM, McCoy CP, Rademacher JT, et al. Signaling Recognition events with fluorescent sensors and switches. Chemical Reviews 1997;97:1515–66.
[9] Valeur B, Leray I. Design principles of fluorescent molecular sensors for cation recognition. Coordination Chemistry Reviews 2000;205:3–40.
[10] Valeur V, Badaoui F, Bardez E, Bourson J, Boutin P, Chatelain A, et al. In: Desvergne JP, Czarnik AW, editors. Chemosensors of ion and molecule recognition. NATO ASI Series. Dordrecht: Kluwer; 1997.
[11] Dujols V, Ford F, Czarnik AW. A long-wavelength fluorescent chemodosimeter selective for Cu(II) ion in water. Journal of the American Chemical Society 1997;119:7386–7.
[12] For review, see: Kim HN, Lee MH, Kim HJ, Kim JS, Yoon J. A new trend in rhodamine-based chemosensors: application of spirolactam ring-opening to sensing ions Chemical Society Reviews 2008;37:1465–72.
[13] Xiang Y, Mei L, Li N, Tong AJ. Sensitive and selective spectrofluorimetric determination of chromium(VI) in water by fluorescence enhancement. Analytica Chimica Acta 2007;581:132–6.
[14] Zhou Z, Yu M, Yang H, Huang K, Li F, Yi T, et al. FRET-based sensor for imaging chromium(III) in living cells. Chemical Communication; 2008:3387–9.
[15] Huang K, Yang H, Zhou Z, Yu M, Li F, Gao X, et al. Multisignal chemosensor for Cr^{3+} and its application in bioimaging. Organic Letters 2008;10:2557–60.
[16] Xiang Y, Tong A. A new rhodamine-based chemosensor exhibiting selective Fe^{III}-amplified fluorescence. Organic Letters 2006;8:1549–52.
[17] Bae S, Tae J. Rhodamine-hydroxamate-based fluorescent chemosensor for Fe^{III}. Tetrahedron Letters 2007;48:5389–92.
[18] Zhang X, Shiraishi Y, Hairi T. Fe(III)- and Hg(II)-selective dual channel fluorescence of a rhodamine-azacrown ether conjugate. Tetrahedron Letters 2008;49:4178–81.
[19] Zhang M, Gao Y, Li M, Yu M, Li F, Li L, et al. A selective turn-on fluorescent sensor for Fe^{III} and application to bioimaging. Tetrahedron Letters 2007;48:3709–12.
[20] Zhang X, Shiraishi Y, Hirai T. A new rhodamine-based fluorescent chemosensor for transition metal cations synthesized by one-step facile condensation. Tetrahedron Letters 2007;48:5455–9.
[21] Xiang Y, Tong A, Jin P, Ju Y. New fluorescent rhodamine hydrazone chemosensor for Cu(II) with high selectivity and sensitivity. Organic Letters 2006;8:2863–6.
[22] Chen X, Jou MJ, Lee H, Kou S, Lim J, Nam SW, et al. New fluorescent and colorimetric chemosensors bearing rhodamine and binaphthyl groups for the detection of Cu^{2+}. Sensors and Actuators B: Chemical 2009;137:597–602.
[23] Zhou Y, Wang F, Kim Y, Kim SJ, Yoon J. Cu^{2+}-selective ratiometric and "off-on" sensor based on the rhodamine derivative bearing pyrene group. Organic Letters 2009;11:4442–5.
[24] Zhang X, Shiraishi Y, Hirai T. Cu(II)-selective green fluorescence of a rhodamine-diacetic acid conjugate. Organic Letters 2007;9:5039–42.
[25] Lee MH, Kim HJ, Yoon S, Park N, Kim JS. Metal ion induced FRET OFF–ON in tren/dansyl-appended rhodamine. Organic Letters 2008;10:213–6.
[26] Zheng H, Qian ZH, Xu L, Yuan FF, Lan LD, Xu JG. Switching the recognition preference of rhodamine B spirolactam by replacing one atom: design of rhodamine B thiohydrazide for recognition of Hg(II) in aqueous solution. Organic Letters 2006;8:859–61.
[27] Lee MH, Wu JS, Lee JW, Jung JH, Kim JS. Highly sensitive and selective chemosensor for Hg^{2+} based on the rhodamine fluorophore. Organic Letters 2007;9:2501–4.

[28] Wu D, Huang W, Duan C, Lin Z, Meng Q. Highly sensitive fluorescent probe for selective detection of Hg^{2+} in DMF aqueous media. Inorganic Chemistry 2007;46:1538–40.
[29] Yang YK, Yook KJ, Tae J. A rhodamine-based fluorescent and colorimetric chemodosimeter for the rapid detection of Hg^{2+} ions in aqueous media. Journal of the American Chemical Society 2005;127:16760–1.
[30] Ko SK, Yang YK, Tae J, Shin I. In vivo monitoring of mercury ions using a rhodamine-based molecular probe. Journal of the American Chemical Society 2006;128:14150–5.
[31] Wu JS, Hwang IC, Kim KS, Kim JS. Rhodamine-based Hg^{2+}-selective chemodosimeter in aqueous solution: fluorescent OFF–ON. Organic Letters 2007;9: 907–10.
[32] Shi W, Ma H. Rhodamine B thiolactone: a simple chemosensor for Hg^{2+} in aqueous media. Chemical Communication; 2008:1856–8.
[33] Zhang X, Xiao Y, Qian X. A ratiometric fluorescent probe based on FRET for imaging Hg^{2+} ions in living cells. Angewandte Chemie International Edition 2008;47:8025–9.
[34] Wu D, Huang W, Lin Z, Ch Duan, He C, Wu S, et al. Highly sensitive multiresponsive chemosensor for selective detection of Hg^{2+} in natural water and different monitoring environments. Inorganic Chemisry 2008;47:7190–201.
[35] Zhan XQ, Qian ZH, Zheng H, Su BY, Lan Z, Xu JG. Rhodamine thiospirolactone. Highly selective and sensitive reversible sensing of Hg(II). Chemical Communication; 2008:1859–61.
[36] Soh JH, Swamy KMK, Kim SK, Kim S, Lee SH, Yoon J. Rhodamine urea derivatives as fluorescent chemosensors for Hg^{2+}. Tetrahedron Letters 2007;48:5966–9.
[37] Yang H, Zhou ZG, Huang KW, Yu MX, Li FY, Yi T, et al. Multisignaling optical electrochemical sensor for Hg^{2+} based on a rhodamine derivative with a ferrocene unit. Organic Letters 2007;9:4729–32.
[38] Suresh M, Shrivastav A, Mishra S, Suresh E, Das A. A rhodamine-based chemosensor that works in the biological system. Organic Letters 2008;10: 3013–6.
[39] Huang W, Song C, He C, Lv G, Hu X, Zhu X, et al. Recognition preference of rhodamine-thiospirolactams for mercury(II) in aqueous solution. Inorganic Chemistry 2009;48:5061–72.
[40] Kwon JY, Jang YJ, Lee YJ, Kim KM, Seo MS, Nam W, et al. A highly selective fluorescent chemosensor for Pb^{2+}. Journal of the American Chemical Society 2005;127:10107–11.
[41] Peng X, Du J, Fan J, Wang J, Wu Y, Zhao J, et al. A selective fluorescent sensor for imaging Cd^{2+} in living cells. Journal of the American Chemical Society 2007;129:1500–1.
[42] Chatterjee A, Santra M, Won N, Kim S, Kim JK, Kim SB, et al. Selective fluorogenic and chromogenic probe for detection of silver ions and silver nanoparticles in aqueous media. Journal of the American Chemical Society 2009;131:2040–1.
[43] Shi W, Sun S, Li X, Ma H. Imaging different interactions of mercury and silver with live cells by a designed fluorescence probe rhodamine B selenolactone. Inorganic Chemisry 2010;49:1206–10.
[44] Chin J, Kim DC, Kim HJ, Panosyan FB, Kim KM. Chiral shift reagent for amino acids based on resonance-assisted hydrogen bonding. Organic Letters 2004;6:2591–3.
[45] Yang XF, Guo XG, Zhao YB. Development of a novel rhodamine-type fluorescent probe to determine peroxynitrite. Talanta 2002;57:883–90.
[46] Lee PF, Yang CT, Fan D, Vittal JJ, Ranford JD. Synthesis, characterization and physicochemical properties of copper(II) complexes containing salicylaldehyde semicarbazone. Polyhedron 2003;22:2781–6.
[47] Anthoni U, Christophersen C, Nielsen PH, Püschl A, Schaumburg K. Structure of red and orange fluorescein. Structural Chemistry 1995;6:161–5.
[48] Shiraishi Y, Sumiya S, Kohno Y, Hirai T. A rhodamine-cyclen conjugate as a highly sensitive and selective fluorescent chemosensor for Hg(II). The Journal of Organic Chemistry 2008;73:8571–4.
[49] Peng T, Yang D. Construction of a library of rhodol fluorophores for developing new fluorescent probes. Organic Letters 2010;12:496–9.
[50] Pal A, Bérubé M, Hall DG. Design, synthesis, and screening of a library of peptidyl bis(boroxoles) as oligosaccharide receptors in water: identification of a receptor for the tumor marker TF-antigen disaccharide. Angewandte Chemie International Edition 2010;49:1492–5.
[51] Wang S, Chang YT. Discovery of heparin chemosensors through diversity oriented fluorescence library approach. Chemical Communication; 2008:1173–5.
[52] Sunahara H, Urano Y, Kojima H, Nagano T. Design and synthesis of a library of BODIPY-based environmental polarity sensors utilizing photoinduced electron- transfer-controlled fluorescence ON/OFF switching. Journal of the American Chemical Society 2007;129:5597–604.
[53] Mello JV, Finney NS. Reversing the discovery paradigm: a new approach to the combinatorial discovery of fluorescent chemosensors. Journal of the American Chemical Society 2005;127:10124–5.
[54] Schneider SE, O'Neil SN, Anslyn EV. Coupling rational design with libraries leads to the production of an ATP selective chemosensor. Journal of the American Chemical Society 2000;122:542–3.
[55] Chen CT, Wagner H, Still WC. Fluorescent, sequence-selective peptide detection by synthetic small molecules. Science 1998;279:851–3.
[56] Czarnik AW. Desperately seeking sensors. Chemistry & Biology 1995;2:423–8.